RELEVANCE OF CME TO THE STRUCTURE OF LARGE-SCALE SOLAR MAGNETIC FIELDS

E. V. IVANOV, V. N. OBRIDKO, E. V. NEPOMNYASHCHAYA and N. V. KUTILINA
Institute of Terrestrial Magnetism, Ionosphere and Radio Wave Propagation, Troitsk, Moscow Region, 142092, Russia

(Received 5 January 1998; accepted 7 October 1998)

Abstract. The relevance of the occurrence rate and location of CME events to two main systems (giant and supergiant) of the large-scale solar magnetic field structure has been investigated. The clustering of CME events and solar flares toward the neutral line of the global field system (neutral line of the source surface field) corroborates the finding by Hundhausen that CME locations track the heliomagnetic equator. A good correlation has been revealed between the CME occurrence rate and variations of the index of the effective solar multipole, that characterizes the typical scale of the global solar magnetic field. The CME rate exhibits sharp jumps/decreases when the index of the effective solar multipole passes through $n = 4$. The observations of X-ray 'blow-out' effects have been analyzed as probable manifestations of CMEs on the disk and have been compared with the large-scale magnetic field structure. As shown by the analysis, the X-ray arcades straddle the neutral line and occur, or at least tend to occur, where the neutral line exhibits a sharp bend. A conclusion is made that CME events are caused by interaction of two large-scale field systems, one of them (the global field system) determining the location of CMEs and another (the system of closed magnetic fields) their occurrence rate.

1. Introduction

A coronal mass ejection (CME) is one the most powerful geoeffective events of solar activity. The origin of CMEs, however, still remains unknown. They are often recorded before the accompanying solar flares or in the absence of flares. The energy of CME is comparable with the energy of major flares. The number of papers dealing with the analysis of the measured properties of CMEs, including their occurrence rates, location relative to the solar disk, angular widths and speeds, is large enough (Kahler, 1992; Gosling, 1993; Hundhausen, 1993; Webb, 1992, 1995, 1997). Some evidence for CME relation to the heliospheric current sheet (HCS), and thus, to the large-scale solar magnetic fields (LSSMF), is available in literature (Hundhausen, 1993; Webb *et al.*, 1997). There are also some simulations of CME as a disconnected magnetic structure (Wu *et al.*, 1997a, b).

In this work, we make an attempt to compare the locations and the occurrence rates of CMEs with the main LSSMF characteristics. As shown earlier by various authors (Bumba, 1970; Bumba *et al.*, 1968, 1969; Ambrož, 1992; McIntosh and Wilson, 1985; Obridko, 1983, 1985; Ivanov, 1986, 1995, 1996), the solar magnetic field is a superposition of several field systems of different space-time scale.

Solar Physics **184:** 369–384, 1999.

Among them, two large-scale field systems can be isolated as most important as for their energy contribution and the role they play in the global organization of various phenomena of solar activity. These systems are likely to be connected in some way or another with the corresponding layers of the large-scale convection, so that, for the sake of brevity, we shall use a conventional term 'cells' for their structural elements. In fact, we have no positive information about the shape of these elements, and can only speak of the typical space scale of the two systems under discussion.

One system, called the global field system, is manifested in the photosphere as typical elements with the size of $70-110^\circ$ and is characterized by a reduced differential rotation. In the photospheric magnetic field, represented as a multipole, this system is manifested as the sectorial component of the global magnetic field of the Sun, that corresponds to the 4-sector structure of the interplanetary magnetic field. There is every reason to believe that it coincides with the system of open magnetic fields that take root deep in the Sun and often emerge at the surface to form cells with a mean characteristic size of 90°. This component of the solar magnetic field is most clearly defined at the source surface. The source-surface field has been assumed at a distance of 2.5 solar radii from the center of the Sun. (The calculation method was described by many authors, e.g., see Hoeksema (1991), Hoeksema and Scherrer (1986), Ivanov, Obridko, and Shelting (1997), Mogilevsky, Obridko, and Shilova (1997)). It is by definition an open field, and its neutral line forms the base of the heliospheric current sheet. The source-surface field can be constructed following the procedure used for spatial filtering of the field, measured in the photosphere, and for isolating the main solar magnetic field at the base of the convection zone.

Another large-scale field system appears in the photosphere as closed magnetic fields with a cell size of $\sim 30-40^\circ$ and is confined to the heliolatitudes of $\pm 50-60^\circ$. It seems to be due to differentially rotating magnetic fields that lie at smaller depths and manifest themselves as the fields of active regions or plages. This group comprises also the local fields of sunspots, but the latter have much smaller typical dimensions and give a relatively smaller contribution to the total magnetic flux of the Sun, than the fields of active regions (Harvey and White, 1996). We believe that the global field is the basic magnetic field in the Sun, all other field systems with a characteristic size of cells less than $\sim 70-90^\circ$ being formed as it rises to the upper layers in the solar atmosphere and interacts with the multi-layer solar convection. The fields with smaller cells are involved in differential rotation of the Sun and form closed field systems.

These field systems and their interaction are considered in more detail in our other papers (Ivanov, 1995, 1996; Obridko and Shelting, 1998). The main objective of this work is to show that CMEs occur as a result of interaction of two systems of magnetic fields (a global system with a characteristic size of cells $\sim 90^\circ$ and a closed field system with a characteristic size of cells $\sim 30-40^\circ$) , and therefore they bear some features characteristic of each of them.

Section 2 contains the data, selected for the analysis. In Section 3, the cyclic variation of the occurrence rate of the global field neutral line at different heliolatitudes is compared with that of heliolatitude distribution of the CME occurrence rate. The clustering of CME events and solar flares of different intensity towards the neutral line of the global field system (neutral line of the source surface field) is described in Section 4. In Section 5, we introduce the index of the effective solar multipole that represents the relative contribution of two large-scale field systems in different phases of the solar cycle. This index is shown to correlate fairly well with the occurrence rate of CME events. Then, in Section 6, we analyze the 'blow-out' observations in X-rays as probable manifestations of CMEs on the disk and compare them with the large-scale magnetic fields structure. In Section 7, we discuss the results and arrive at the conclusion that CME events are caused by interaction of two large-scale field systems. One of them (the global field system) determines the location of CMEs and another (the system of closed magnetic fields) their occurrence rate.

2. Observation Data

To compare CME and LSSMF, we have used the maps of solar magnetic fields, calculated for the source surface ($r = 2.5$ solar radii) under potential approximation (for details see Hoeksema (1991), Hoeksema and Scherrer (1986), Ioshpa, Mogilevsky, and Obridko (1997), Ivanov, Obridko, and Shelting (1997), Mogilevsky, Obridko, and Shilova (1997), etc.) and the catalogues of CME data from the Solar Maximum Mission satellite (Burkepile and St. Cyr, 1993), P78-1 (Howard *et al.*, 1991), and from the ground-based Mauna Loa Solar Observatory in Hawaii (MLSO)). The list of activity for years 1991–1995 from MLSO was obtained by INTERNET. We have only used the events, reported by the observers as connected with CME. The data from SMM proved most reliable. The data from P78-1 and MLSO were only used to fill the gaps in the SMM data (1979, 1981-1983, 1991-1995) and to make a qualitative comparison with SMM results.

A comparison of CME data from SMM and P78-1 for the time intervals, when observations were done on both satellites, revealed some systematic differences, that concerned, first of all, the estimates of CME widths and, to a smaller extent, their apparent latitudes. The data from MLSO are scarce and do not practically contain estimates of CME widths. We have only used them to estimate the clustering of CME events towards the neutral line of the global magnetic field during 1991–1995. The systematic differences between the SMM and P78-1 data are discussed below.

3. Cycle Variation of the Heliolatitude Distribution of CMEs

Hundhausen (1993) studied the heliolatitude distribution of CMEs during one solar cycle. It proved to be quite specific. Near the minimum of the cycle, all CME are clustered in a narrow heliolatitude zone near the equator. At the maximum of the cycle, they are widely spread from one pole to another. The distribution of CMEs and its variations with the phase of the solar cycle differs fundamentally from the behaviour of the sunspots (Maunder butterflies), pointing to a possible relation of CME to the global structure of solar magnetic fields.

This hypothesis was checked as follows. In addition to the Hundhausen's statistical data, we have calculated the relative index of presence of the global field neutral line at a given latitude for each year – the annual occurrence rate of the global field neutral line at a given latitude in the northern and southern hemispheres, calculated from the source surface field maps.

In Figure 1, the histogram of the relative index of the presence of the global field neutral line at a given latitude for each year is superimposed on the distribution of CME occurrence rates (dotted line), obtained by Hundhausen. Unlike the distribution of CME occurrence rates, that occupies a heliolatitude interval of $\pm 90^\circ$, the histograms of the relative index of the presence of the global field neutral line at a given latitude are confined to $\pm 70^\circ$. This is because due to the perspective shortening, the observations of photospheric magnetic fields and the estimates of the source surface neutral line are not available at higher latitudes. A good agreement of these distributions suggests a relationship between the CME location and the neutral line of the global magnetic field, i.e., the first (global) large-scale field system.

4. Clustering of Solar Flares and CMEs towards the Global Magnetic Field Neutral Line and its Variations with the Solar Cycle

Bumba and Obridko (1969) discovered the effect of clustering of active regions with proton flares towards the IMF sector boundaries. Later, this result was many times validated by the authors and by other investigators (Obridko, Mansurov, and Mansurova, 1974; Levitsky, 1980; Obridko and Starkova, 1981; Stepanyan, 1982; Stewart and Bravo, 1996). It proved to be the more pronounced, the more powerful events were considered. The CMEs being justly considered a global analog of flares, it was interesting to try to reveal a similar effect for CMEs and to compare it with observations of the flare-active regions.

Two parameters were determined for all CMEs and flares:

Δ – the shortest distance along the normal from the CME center or flare to the nearest point on the neutral line of the global solar magnetic field (i.e., the neutral line of the source-surface field); and $\Delta\lambda$ – the distance from the CME center or flare to the nearest IMF sector boundary (intersections of the neutral line

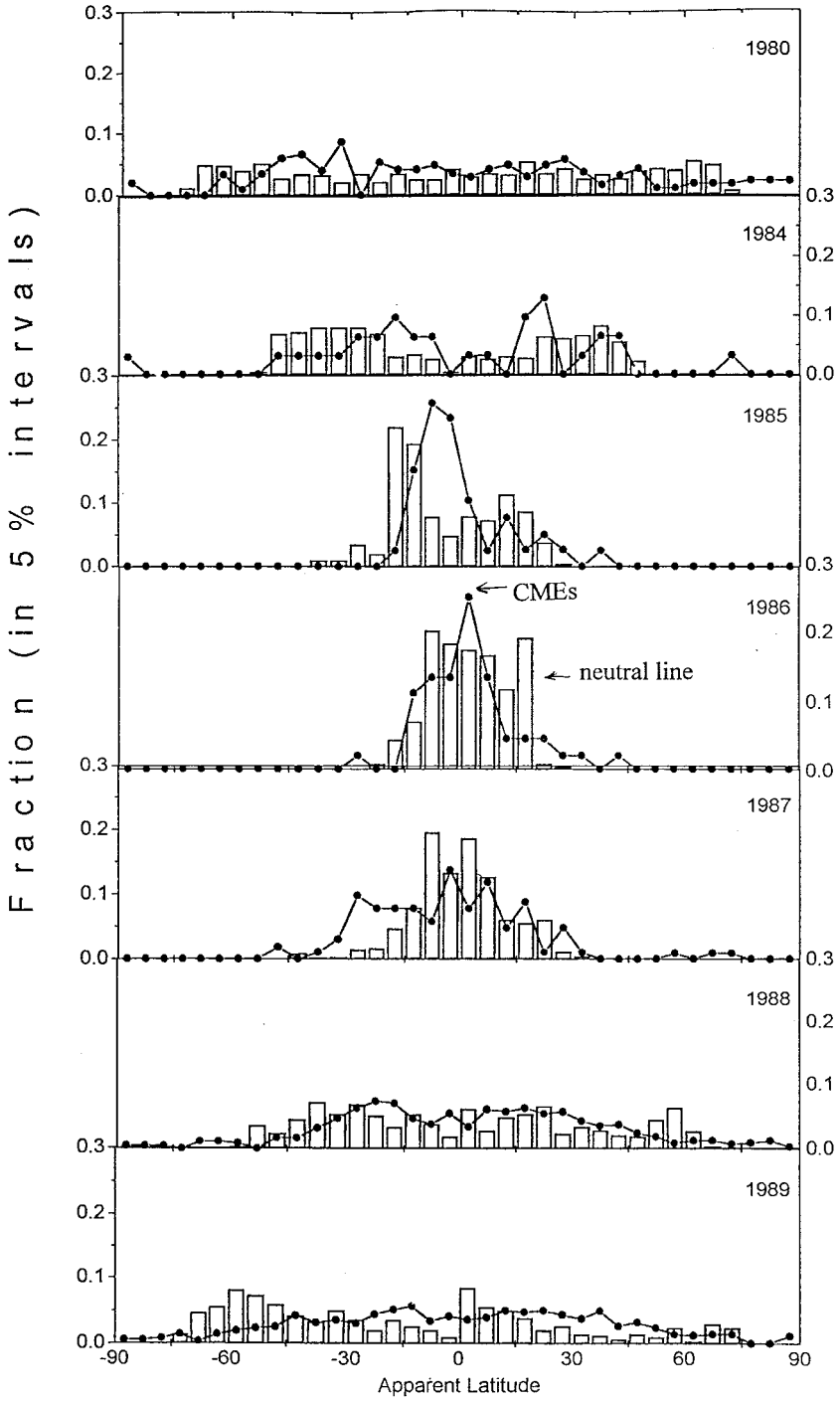

Figure 1. Relative index of the presence of the global field neutral line at a given latitude for each year (histogram) superimposed on the distribution of CME occurrence rates, obtained by Hundhausen (1993) (dotted line).

of the source-surface field with the plane of ecliptic), as was usually done in the previous work (Bumba and Obridko, 1969; Obridko, Mansurov, and Mansurova, 1974; Levitsky, 1980; Obridko and Starkova, 1981). CME locations were determined by the method proposed by Burkepile and St. Cyr (1993). The central angle of the projection of CME position angle onto the plane of the sky was taken as the CME heliolatitude (the central angle being the geometric center between the two outermost sides of the feature to be identified). For the CME heliolongitude, we took the longitude of the solar limb, on which the CME was observed on the day of its occurrence. Of course, the contribution of the off-limb non-equatorial features made us overestimate the actual latitude and longitude. However, this contribution was significantly reduced by averaging as the annual mean values of Δ and $\Delta\lambda$ were calculated. Besides, such overestimation can not result in a fictitious dependence on the phase of the solar cycle. So, we have reason to believe that the observed cyclic variation of CME clustering towards the neutral line of the global magnetic field is a real phenomenon, that reflects periodic variations of the system of large-scale magnetic fields (under the assumption of a relationship between CME and the large-scale field structure).

In the statistical sense, both values lead to similar results, so that in further considerations we used only the distance, Δ.

Figure 2(a) illustrates the annual mean distances of CME from the neutral line of the global magnetic field in heliographic degrees with their r.m.s. errors. Solid lines show the third-order polynomial fits for the SMM and P78-1 CME data bases, and a square fit for the MLSO CME data base. In spite of different reliability of data and different observation methods, all three data series point clearly to CME clustering towards the neutral line of the global magnetic field and, therefore, to a close relationship of CME with the global magnetic field of the Sun. Note that the mean CME distance at the minimum of the cycle is much smaller than at the maximum. It is probably indicative of a more intimate relation of CMEs to the global magnetic field of the Sun at the minimum of the solar cycle, when the system of closed magnetic fields is weak or nonexistent.

CME data from SMM and P78-1 reveal the same character of cyclic variations of CME clustering towards the global field neutral line. Systematic differences in the degree of concentration (stronger clustering of CMEs towards the neutral line of the global field from the P78-1, than from the SMM data during 1980–1985) are obviously due to different instrumental facilities of the satellites and different recording procedures.

Figure 2(b) shows the mean distance to the neutral line of the global magnetic field, Δ, for flares (separately for proton flares and for all flares of importance $>$1B). The fifth-order polynomial fits for all flares of importance $>$1B are plotted by a solid curve and the third-order polynomial fits for proton flares by a dashed curve. As seen from Figures 2(a) and 2(b), the difference between the mean distances, Δ, for the flares and CMEs falls within the error limits, and their dependence on the solar cycle is the same. The similarity of the curves for flares

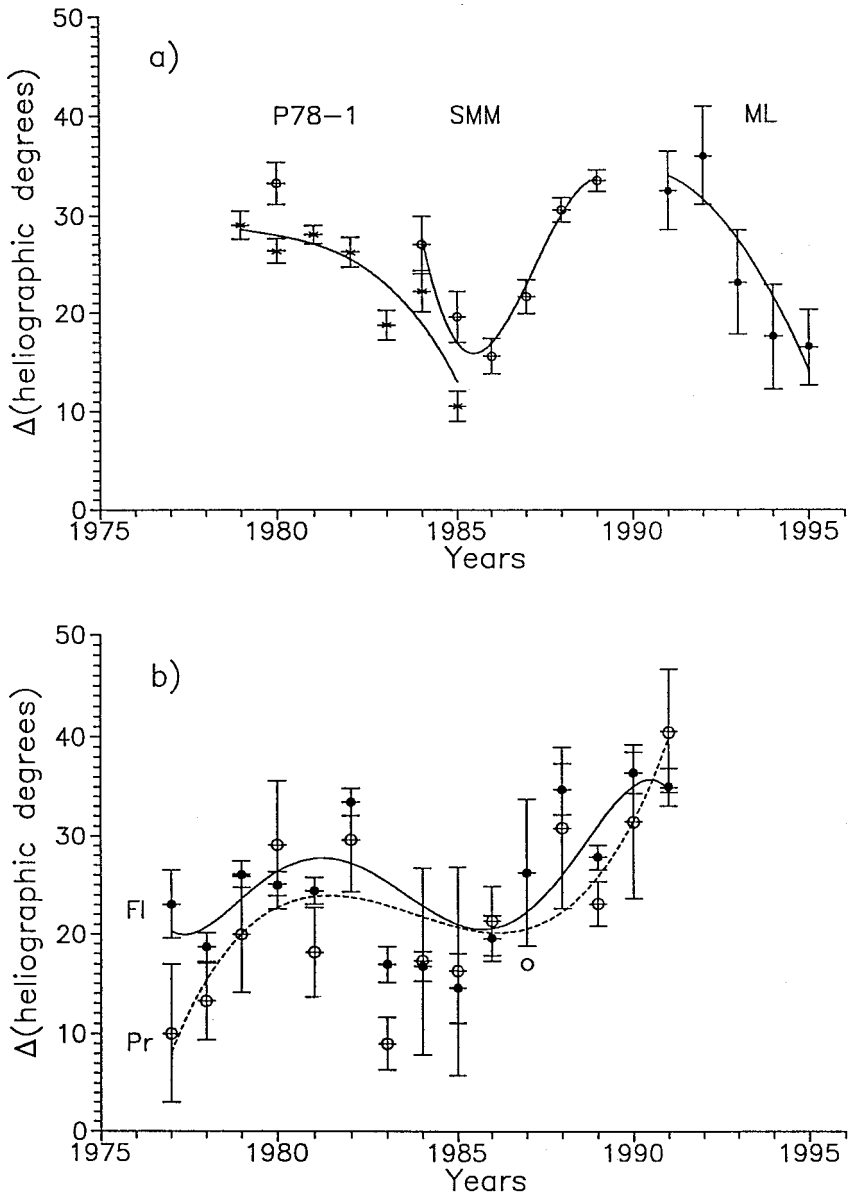

Figure 2. (a) The annual mean distance from the center of CME to the neutral line of the global magnetic field in heliographic degrees (open circles – SMM, asterisks – P78-1, filled circles – MLSO). (b) The mean distance to the neutral line of the global magnetic field, Δ, separately for proton flares (open circles) and for all flares of importance >1B (filled circles).

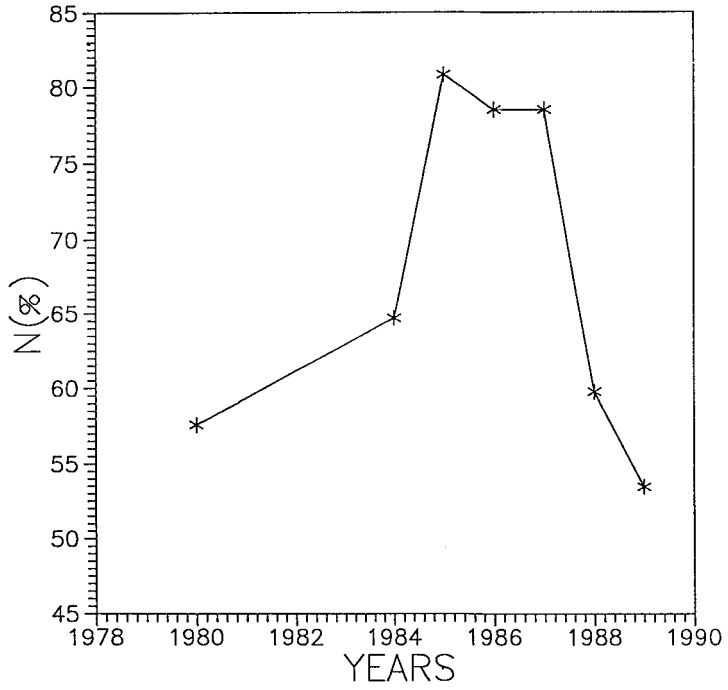

Figure 3. The relative number of CME events, observed within 30° ($\sim \frac{1}{3}$ a supergiant cell) from the global field neutral line.

and for CMEs in Figures 2(a) and 2(b) lends credibility to the CME curve, because, unlike CMEs, the latitude and longitude of the flares are well determined.

Figure 3 illustrates the relative number of CMEs, observed within 30° from the global field neutral line. The 30° distance from the neutral line of the global magnetic field is small compared to the 90° scale size of the global magnetic field (characteristic size of the supergiant cell). One can see that the CME concentration towards the global magnetic field neutral line within the 30° zone from the neutral line is always higher than 50%, exceeding 80% at the minimum of the cycle.

5. Relationship between CMEs and the Index of the Large-Scale Solar Structure, n (the Index of Effective Solar Multipole)

To characterize the energy of the large-scale magnetic field of the Sun, Obridko and Ermakov (1989) introduced the energy index of the large-scale magnetic field, $i(B_r) = \langle B^2 \rangle$, on a surface of radius r, where $\langle B^2 \rangle$ is the square intensity of the magnetic field radial component averaged over the solar surface, and r is the radius of the sphere, over which the field is averaged. When passing from the photosphere and lower corona ($r < 1.5\ R_0$), with the prevailing closed configuration of magnetic field, to the upper corona ($r > 1.5\ R_0$), with the prevailing open configuration,

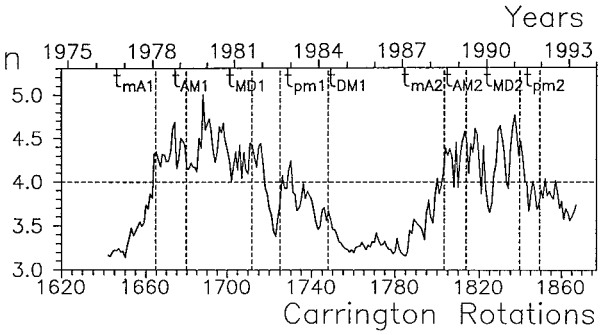

Figure 4. Variation of the index of the effective solar multipole, n, during solar cycles 21 and 22.

the behaviour of the $i(B_r)$ index changes noticeably. Let us introduce the index of effective solar multipole, n, to estimate the contribution of different components of the large-scale magnetic field at various stages of the 11-year solar cycle:

$$n = -0.5 \log(I_{ss}/I_{ph})/\log(2.5) \ .$$

This index is determined by taking the logarithm of the ratio of the $i(B_r)$ value at the source surface, I_{ss}, to that in the photosphere, I_{ph} (Ivanov, Obridko, and Shelting, 1997). In fact, when passing from the photosphere to the source surface, the magnetic flux changes in accordance with the equation $B_{ss} = B_{ph} r^{-n}$, where $n = 3$ for a dipole source, $n = 4$ for a quadrupole source, and $n > 4$ for a higher-order multipole source. When the field under consideration is a combination of the fields of different sources with different weights, n can assume different values from 3 to 4 (in the case of combined dipole and quadrupole sources) or higher (in the case of a higher-order multipole field). Figure 4 illustrates variations of n during solar cycles 21 and 22. As seen from the figure, (i) there is no phase, when a purely dipole source is present, always $n > 3$; (ii) the multipole component at the source surface becomes significant in the growth phase (for $n > 4$), remains significant during the whole maximum phase and the most part of the declining phase, and turns insignificant by the time of the transition to the cycle minimum.

Figure 4 also illustrates the reference points of the solar cycle, t_{mA}, t_{AM}, t_{MD}, t_{pm}, and t_{Dm}. These points were introduced earlier by Vitinsky *et al.* (1986) and Obridko and Shelting (1993) to mark the beginning and the end of the phases of the solar cycle: t_{Dm} and t_{mA} – the beginning and end of the minimum epoch, t_{AM} and t_{MD} – the beginning and end of the maximum, and t_{pm} – a pre-minimum. Usually they coincide with the pronounced local maxima of the cyclic curves of various solar indices, as well as with the maxima of the cyclic curve of the large-scale field energy index, $i(B_r)$.

As seen from Figure 4, these points coincide also with the noticeable peaks of the n index, that describes structural variations of the large-scale solar magnetic field. Ivanov (1995, 1996) showed that the reference points occurred where the system of supergiant cells (with a characteristic size of $\sim 90°$) displayed changes,

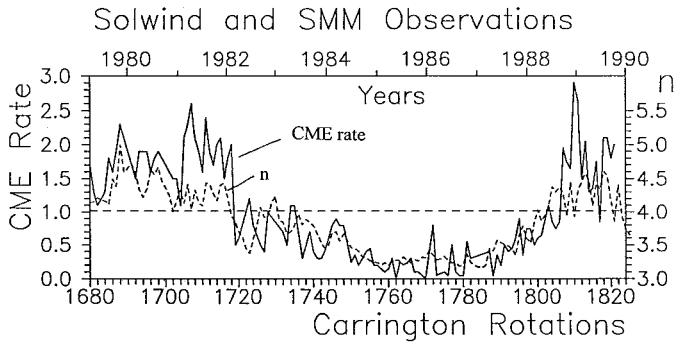

Figure 5. Cyclic variation of the index of the effective solar multipole, n (dashed line), and the rotation-averaged CME occurrence rate (Cliver *et al.*, 1994) (solid line).

accompanied by the corresponding changes in the shape of the solar corona and the HCS large-scale structure.

The multipole component corresponds to the hierarchy of fields with a typical size of the cells $D \lesssim 40{-}60^\circ$ ($D < 0.5\ R_0$), whose magnetic flux decreases rapidly with height and does not usually reach the source surface. Therefore its increasing contribution at the maximum of the cycle implies redistribution of energy of the large-scale magnetic field between the systems of open and closed fields, and activation of the latter. Redistribution of energy between the field's open and closed configurations (the former including polar fields and supergiant cells in the equatorial zone, and the latter the giant and smaller-scale cells) occurs at the moments corresponding to the reference points, t_{mA}, t_{AM}, t_{MD}, t_{pm}, and t_{Dm}. This implies a change of the activity regime and a transition from one phase of the solar cycle to another.

In Figure 5, variations of the index of effective solar multipole, n, are juxtaposed with variations of the rotation-averaged CME rate (Cliver *et al.*, 1994). The comparison reveals an amazing similarity of both curves, which indicated to a close relationship between both variations. Activation of the system of giant cells, accompanied by increased contribution of the multipole global field component to the source surface magnetic flux ($n > 4$), results in an increase of CME occurrence rate, and vice versa, a decrease of n ($n < 4$) results in a similar decrease of CME occurrence rate. A close relationship between CME and a system of giant cells is corroborated by the fact that the typical mean CME size is $\sim 40^\circ$ and does not depend on the phase of the cycle. Besides, the occurrence zones of CME and the system of giant cells change synchronously during the solar cycle (Hundhausen, 1993).

6. *Yohkoh* X-Ray Observations of the 'Blow-Out' Effect as a Probable Manifestation of CME Occurrence at the Periphery of Coronal Holes

Bhatnagar (1996, 1997) described SXT *Yohkoh* observations of the 'blow-out' effect, regarding it as the initial phase of CME evolution. This allows us to analyze the magnetic field structure directly at the CME occurrence site.

The analysis procedure applied here is as follows. For each of the 15 events, tabulated by Bhatnagar (1996, 1997), we have constructed a complex figure, consisting of the following parts:

(a) SXT *Yohkoh* image, obtained on a given day, but usually not at the same time as 'blow-out' was observed.

(b) Spherical image of the Sun with superimposed map of the radial magnetic field component at the source surface (2.5 solar radii) and a system of *open* field lines.

(c) Spherical image of the Sun with superimposed radial component of the photospheric magnetic field. In the same picture are also plotted all field lines that originate in the photosphere. Here, most of the area at the photospheric level is occupied by closed configurations.

(d) Spherical image of the Sun with superimposed line-of-sight magnetic field component, calculated at the height of 1.3 solar radii.

(e) The central part of synoptic map with the plotted vectors of the transverse magnetic field component, calculated at 1.3 solar radii.

In some cases, we plotted the calculated image (radial field plus field lines) over the SXT image.

It is important to note that the field structure in items (b–e) was not measured, but calculated under potential approximation using 9 terms of expansion. As shown by Obridko, Kharshiladze, and Shelting (1995a, b), this means that the field on the maps is primarily large-scale, and the neutral line belongs to the large-scale field. In fact, the calculation process involves a kind of filtering to reduce the effect of local fields. Thus, we are sure to compare SXT images with the large-scale field structure, unlike in the papers by Bhatnagar (1996, 1997), where the comparison was made with the directly measured field.

Unfortunately, space limitations do not allow us to illustrate here all magnetic field configurations, listed above. By way of example, we give in Figure 6 a *Yohkoh* SXT image for 3 October 1993, a figure from Bhatnagar (1996) with the 'blow-out' locations shown with hatching, and the magnetic field calculated as described in items (c) and (b). One can see an arch system in the vicinity of the 'blow-out'.

The results of the analysis of all 15 events can be summarized as follows:

(1) The conclusions of Bhatnagar are corroborated: the X-ray 'blow-out' events occur at the periphery of coronal holes.

(2) In all cases, when we knew exact location of the X-ray 'blow-outs', they either occurred right on the neutral line of the large-scale magnetic field radial component, or near it, within the same magnetic arch structure. These are the places

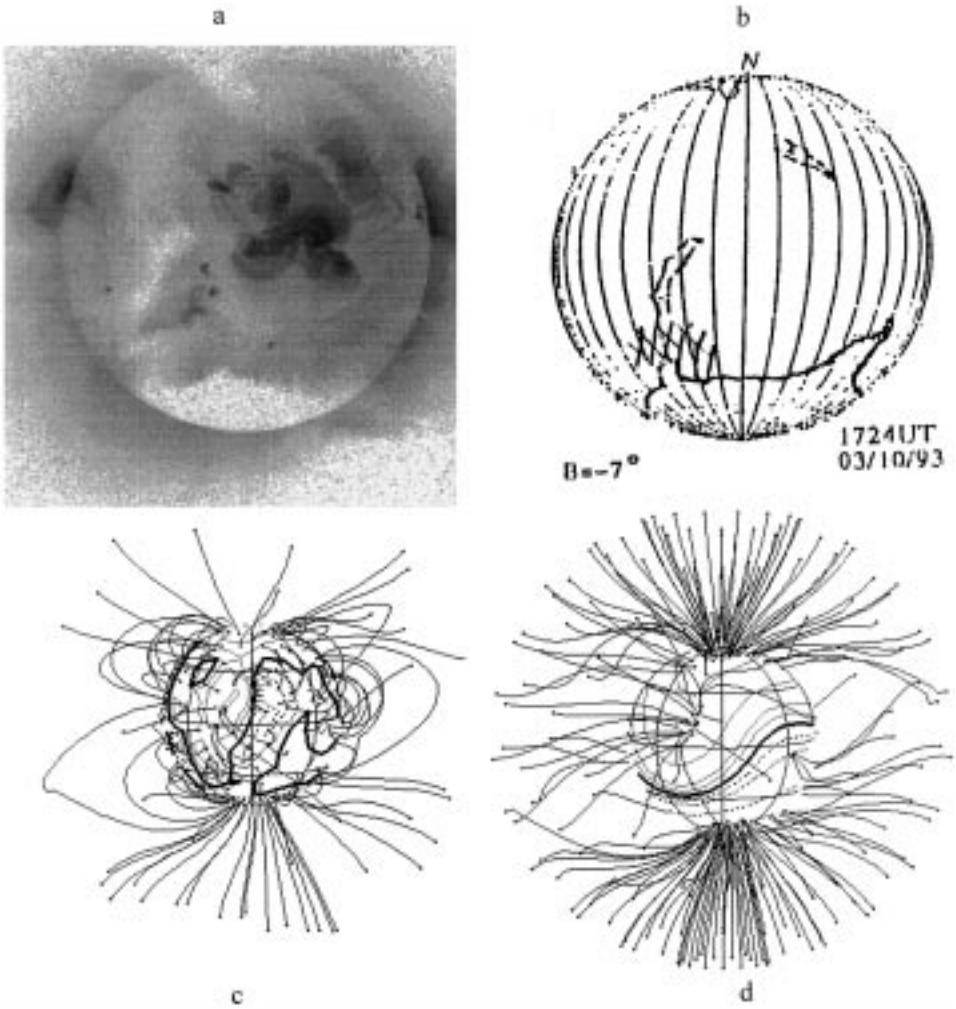

Figure 6. Comparison of the observed phenomena with the calculated magnetic field for October 3, 1993. (a) *Yohkoh* SXT image; (b) Figure from the paper by Bhatnagar (1996) with the 'blow-out' locations. (c) Spherical image of the Sun with superimposed radial component of the photospheric magnetic field and all field lines that originate in the photosphere; here, most of the area at the photospheric level is occupied by *closed* configurations; (d) Spherical image of the Sun with superimposed map of the radial magnetic field component at the source surface (2.5 solar radii) and a system of *open* field lines.

where the neutral line often displays a sharp bend or the patches of opposite field polarity are observed. Similar results are reported by Webb *et al.* (1997)

(3) In all cases, when the X-ray 'blow-out' event appears as an elongated object, it extends along the neutral line of the large-scale magnetic field.

(4) The magnetic field below and near the X-ray 'blow-out' has the form of an arch system (arcade or tunnel) under the neutral line. The arches are often

strongly tilted, so that the transverse field at both ends of the field line has the same direction along the neutral line. Though our calculations were performed under currentless approximation, the real field structure at this place seems to display a shear effect, which agrees fairly well with the *Yohkoh* and MLSO observations (Hiei, Hundhausen, and Sime, 1993; Klimchuk *et al.*, 1994).

(5) Once appearing, the X-ray 'blow-out' event seems to propagate along the neutral line, and then, upwards. This differs from the traditional propagation scheme of emission in a two-ribbon Hα flares, where the ribbons usually diverge from the neutral line.

(6) The scenario of the X-ray 'blow-out' evolution and subsequent coronal mass ejection is similar to that of generation and evolution of a solar flare. The main difference is that the flare occurs in local fields of active regions, whereas the event under consideration occurs in large-scale global fields. Both events are characterized by their location near the respective neutral line, in the region of large gradients and intensive transverse fields with a probable shear effect. However the different scale of the fields results in a different scale of events, in a more powerful mass ejection, in propagation of disturbance along the arcade, and disappearance of the large-scale filament. As shown in our earlier work, coronal holes tend to occur inside the bays and bends of the neutral line (Obridko and Shelting, 1989, 1990).

It should be noted that CMEs are observed at the periphery of the coronal holes, rather than inside them. Webb *et al.* (1978) were the first to report the tendency of CMEs/magnetic arcades to originate at the boundaries of coronal holes. As shown by Mogilevsky, Obridko, and Shilova (1997) and Obridko and Shelting (1998), they occur in the transition zone between the neutral line of the source-surface field and the open-field region (coronal hole). It is obvious that the occurrence of coronal holes is due to a specific structure of the large-scale magnetic field. Once arising, a CME may cause some deformation of the magnetic field structure and even result in the occurrence of a short-lived coronal hole at the very site of the CME origin. However the basic arch structure of the field exists usually before the CME event starts. This conforms with the idea that CMEs proceed from large-scale closed magnetic structures, put forward by Hundhausen (1993) and Webb *et al.* (1997).

7. Discussion of Results

All said in the previous sections leads us to the conclusion that both systems of large-scale magnetic fields, described above, play an important role in generation of CMEs. Here we must again remember the similarity of events in local fields of active regions and in large-scale magnetic fields (Obridko, 1997; Obridko and Shelting, 1998).

The main objects in an active region are sunspots, i.e., relatively small features with a strong quasi-vertical field. The sunspot groups usually consist of sunspots of different polarity, separated by a neutral line. The space between the sunspots and the neutral line is filled with the penumbra and plages, in which the field has a significant tangential component. Solar flares rarely occur in the sunspot umbra, but are rather localized in the penumbra and plages in the vicinity of the neutral line. During a flare, one can often observe the regions of inter-crossed transversal fields ('*bifurcations*') and a shear.

Now, let us turn our attention to the large-scale fields. Coronal holes resemble sunspots in many respects (see Obridko and Shelting, 1998, and references therein). They occur at the peaks of quasi-radial global field of open configuration. Like sunspots, they usually appear in 'bipolar groups'. The coronal holes of different polarity are separated by the neutral line of the global magnetic field, that is not observed directly, but is calculated as the neutral line at the source surface – the base of the heliospheric current sheet. Sometimes it is also called the magnetic equator. These are the elements of the first field system. Between coronal holes and the neutral line, interacting and somewhat distorting them, there are closed fields of the second field system. This is the region, where CME occur at the periphery of coronal holes and in the vicinity of the neutral line. This is the apparent contradiction, inherent in CME events: they are generated by the second field system, though in the developed state they appear as elements of the first – global field system. They are closely linked to the global field features, such as coronal holes and magnetic equator.

Thus, the occurrence rate and location of CMEs is determined by interaction of both systems of the large-scale magnetic field, the occurrence rate being determined by the second system and the location by the first one.

Acknowledgements

The work was supported by the Russian Foundation for Basic Research (Projects No. 98–02–16189, 96–02–17054, and 07–02–1691) and the National Program for Astronomy. The authors would like to thank the referee for valuable remarks.

References

Ambrož, P.: 1992, in S. Fisher and M. Vandas (eds.), *Proceedings of the First SOLTIP Symposium* **21**, 38.

Bhatnagar, A.: 1996, *Astrophys. Space Sci.* **243**, 105.

Bhatnagar, A.: 1997, *SOLTIP III Symposium in China*, Beijing (in press).

Bumba, V.: 1970, *Solar Phys.*, **2**, 80.

Bumba, V. and Obridko, V. N.: 1969, *Solar Phys.* **6**, 104.

Bumba, V., Howard, R., and Smith, S. F.: 1964, *Carnegie Inst. Washington Year Book* **63**, 6.

Bumba, V., Howard, R., Martres, M. J., and Soru-Iscovici, J.: 1968, 'Structure and Development of Solar Active Regions', *IAU Symp.* **35**, 13.
Bumba, V., Howard, R., Kopecký, M., and Kuklin, G. V.: 1969, *Bull. Astron. Inst. Czech.* **20**, 18.
Burkepile, J. T. and St. Cyr, O. C.: 1993, *A Revised and Expanded Catalogue of Mass Ejections Observed by the Solar Maximum Mission Coronagraph*, High Altitude Obs., Natl. Cent. for Atmos. Res., Boulder, Colo.
Cliver, E. V., St. Cyr, O. C., Howard, R. A., and McIntosh, P. S.: 1994, in V. Rušin, P. Heinzel, and J.-C. Vial (eds.), *IAU Colloq.* **144**, 83.
Gosling, J. T.: 1993, *J. Geophys. Res.* **98**, 937.
Harvey, K. L. and White, O. R.: 1996, SPRC Technical Report 96–01.
Hiei, E., Hundhausen, A. J., and Sime, D. G.: 1993, *Geophys. Res. Lett.* **20**, 2785.
Hoeksema, J. T.: 1991, Report CSSA-ASTRO-91-01.
Hoeksema, J. T. and Scherrer, P. H.: 1986, WDCA, UAG Report 94, Boulder, USA.
Howard, R. A., Sheeley, N. R. Jr., Koomen, M. J., and Michels, D. J.: 1991, *Preliminary CME List*, Washington.
Hundhausen, A. J.: 1993, *J. Geophys. Res.* **98**(A8), 13177.
Ivanov, E. V.: 1986, *Soln. Dann.* No. 7, 61.
Ivanov, E. V.: 1995, *Bull. Russian Acad. Sci., Physics* **59**(7), 1133.
Ivanov, E. V.: 1996, *J. Geomag. Geoelectr.* **48**(1), 11.
Ivanov, E. V., Obridko, V. N., and Shelting, B. D.: 1997, *Astron. Reports* **41**(2), 236.
Kahler, S. W.: 1992, *Ann. Rev. Astron. Astrophys.* **30**, 113.
Klimchuk, J. A., Acton, L. W., Harvey, K. L., Hudson, H. S., Kluge, K. L., Sime, D. G., Strong, K. T., and Watanabe, T.: 1994, in Y. Uchida *et al.* (eds.), *X-ray Solar Physics from Yohkoh*, Universal Academy Press, Tokyo, p. 181.
Levitsky, L. S.: 1980, *Izv. Krymsk. Astrofiz. Obs.* **62**, 148.
McIntosh, P. S. and Wilson, P. R.: 1985, *Solar Phys.* **97**, 59.
Mogilevsky, E. I., Obridko, V. N., and Shilova, N. S., 1997, *Solar Phys* **176**, 107.
Obridko, V. N.: 1983, *Publ. Debrecen Heliophys. Obs.* **5**(1), 25.
Obridko, V. N.: 1985, *Sunspots and Activity Complexes*, Nauka, Moscow.
Obridko, V. N.: 1997, *SOLTIP III Symposium in China*, Beijing (in press).
Obridko, V. N. and Ermakov, F. A.: 1989, *Astron. Circ.* **1539**, 24.
Obridko, V. N. and Kuklin, G. V.: 1993, in J. Hruška, M. A. Shea, D. F. Smart, and G. Heckman (eds.), *Solar-Terrestrial Predictions, IV*, Proc. Workshop at Ottawa, Canada, May 18–22: 1992, **2**, p. 273.
Obridko, V. N. and Starkova, L. I.: 1981, *Problems of Space Electrodynamics*, IZMIRAN, Nauka, p. 29.
Obridko, V. N. and Shelting, B. D.: 1992, *Solar Phys* **137**, 167.
Obridko, V. N. and Shelting, B. D.: 1989, *Solar Phys.* **124**, 73.
Obridko, V. N. and Shelting, B. D.: 1990, *Astron. Zh.* **67**, 890.
Obridko, V. N. and Shelting, B. D.: 1998, *Solar Phys.* **184**, 187.
Obridko, V. N., Kharshiladze, A. F., and Shelting, B. D.: 1995a, *Astron. J.* **72**, 108.
Obridko, V. N., Kharshiladze, A. F., and Shelting, B. D.: 1995b, *Astron. Astrophys. Transactions* **9**, 1.
Obridko, V. N., Mansurov, S. M., and Mansurova, L. G.: 1974, *Geomagn. Aeron.* **14**(1), 3.
Stewart, G. A and Bravo, S.: 1996, *Adv. Space Res.* **17**(4–5), 217.
Vitinsky, Yu. I., Kuklin, G. V., and Obridko, V. N.: 1986, *Soln. Dann.* No. 3, 53.
Webb, D. F.: 1992, in Z. Švestka, B. Jackson, and M. Machado (eds.), *Eruptive Solar Flares*, Springer-Verlag, New York, p. 234.
Webb, D. F.: 1995, *Rev. Geophys. Suppl.* **33**, 577.

Webb, D. F.: 1997, in E. Sagawa and M. Akioka (eds.), *Workshop on Solar Flares and Related Disturbances*, Proceedings of a Workshop at Hitachi, Japan, January 23–25, 1996, Hiraiso Solar Terrestrial Research Center, 85.

Webb, D. F., Nolte, J. T., Solodyna, C. V., and McIntosh, P. S.: 1978, *Solar Phys.* **58**, 389.

Webb, D. F., Kahler, S. W., McIntosh, P. S., and Klimchuk, J. A.: 1997, *J. Geophys. Res.* **102**, 24161.

Wu, S. T., Guo, W. P., Andrews, M. D., Bruekner, G. E., Howard, R. A., Koomen, M. J., Korendyke, C. M., Michels, D. J., Moses, J. D., Socker, D. G., Dere, K. P., Lamy, P. L., Liebaria, A., Bout, M. V., Simnett, G. M., Bedford, D. K., and Eyles, C. J.: 1997a, *Solar Phys.* **175**, 719.

Wu, S. T., Guo, W. P., Michels, D. J., Andrews, M. D., Bruekner, G. E., Howard, R. A., Koomen, M. J., Korendyke, C. M., Moses, J. D., Socker, D. G., Dere, K. P., Jean-Lois Bougeret, Lamy, P. L., Schwenn, R., and Simnett, G. M.: 1997b, 'The Corona and Solar Wind near Minimum Activity', *Proceedings of the Fifth SOHO Workshop*, Oslo, Norway, 17–20 June 1997 ESA SP-404, 739.